INTECH
open science | open minds

OPEN ACCESS
ARTICLE

International Journal of Advanced Robotic Systems

Modelling and Experimental Evaluation of a Static Balancing Technique for a new Horizontally Mounted 3-UPU Parallel Mechanism

Regular Paper

Maryam Banitalebi Dehkordi[1], Antonio Frisoli[1,*], Edoardo Sotgiu[1] and Massimo Bergamasco[1]

1 PERCRO, TeCIP Institute, Scuola Superiore Sant'Anna
* Corresponding author E-mail: a. frisoli@sssup. it

Received 11 May 2012; Accepted 02 Oct 2012

DOI: 10. 5772/54009

Abstract This paper presents the modelling and experimental evaluation of the gravity compensation of a horizontal 3-UPU parallel mechanism. The conventional Newton-Euler method for static analysis and balancing of mechanisms works for serial robots; however, it can become computationally expensive when applied to the analysis of parallel manipulators. To overcome this difficulty, in this paper we propose an approach, based on a Lagrangian method, that is more efficient in terms of computation time. The derivation of the gravity compensation model is based on the analytical computation of the total potential energy of the system at each position of the end-effector. In order to satisfy the gravity compensation condition, the total potential energy of the system should remain constant for all of the manipulator's configurations. Analytical and mechanical gravity compensation is taken into account, and the set of conditions and the system of springs are defined. Finally, employing a virtual reality environment, some experiments are carried out and the reliability and feasibility of the proposed model are evaluated in the presence and absence of the elastic components.

Keywords 3-UPU parallel manipulator, gravity compensation, Lagrangian method, experimental test, elastic system

1. Introduction

The translational 3-UPU parallel mechanism has attracted the attention of many researchers for decades. This kind of manipulator has the potential to be used widely in different fields of science and industry, due to its purely translational and precise motion. A great deal of work has been done on several aspects and applications of parallel mechanisms (see, for example, [1-4]). Like other parallel robots, a 3-UPU parallel mechanism provides high load-carrying capacity, high velocity, structural stiffness, precision and low inertia, at the expense of limited

workspace and difficulties with mechanical design, motion generation, direct kinematics and control.

A 3-UPU parallel mechanism exhibits a pure translational motion if the two outer revolute joint axes in each limb are parallel and the two inner revolute joint axes are parallel to one another. Tsai and Joshi carried out one of the first studies on the spatial 3-UPU parallel manipulator, analysing its kinematic properties[5, 6]. Research was further generalized by Frisoli et al. [7], who analysed the geometrical conditions for type synthesis of fully translational parallel manipulators. In 2001 Park introduced a model of 3-UPU parallel manipulator that had an unexpected mobility despite none of the prismatic joints being actuated, and Han et al. carried out the kinematic sensitivity analysis of this robot [8, 9]. This mechanism was later investigated in successive articles interpreting the robot behaviour through several approaches [10, 11]. Walter et al. carried out a complete analysis of the kinematic behaviour of this robot using methods from algebraic geometry [9, 12]. Gregorio and Parenti-Castelli gave an account of the singularities analysis of the translational 3-UPU parallel mechanism, and addressed both translational and rotational singularities [13].

All of the above-mentioned studies addressed the vertically established parallel manipulators –when the robot's base is parallel to the ground and the links are approximately orthogonal to the ground with some degrees of deviation. In these robots the gravity vector is normally directed to the base of the mechanism, which as some advantages in terms of the mechanical compensation of gravity, since the weight of the platform is almost uniformly distributed among the different limbs. In addition, the vertical component of the actuator force is much higher than its horizontal component as it corresponds to the gravitational force; therefore, the actuator's force can efficiently compensate the mechanism's weight. In the case of a horizontally established parallel manipulator, where the limbs are nearly parallel to the ground and the gravity vector lies in the plane of the base, the component of actuator force corresponding to gravitational force is much smaller than the orthogonal one (parallel to ground). This fact seems to become critical in large mechanisms, and the compensation of the high gravitational force through the small vertical component of the actuators' force poses a challenge of gravity compensation for thee manipulators that has not yet been brought into focus.

Gravity compensation and dynamic balancing have been of great interest to researchers for several decades [14-19]. Gravity compensation is known as the condition in which the mechanism is statistically balanced. The literature shows that mainly springs and counterweights, and in a few cases pulleys and cams have been employed in efforts towards gravity compensation for serial mechanisms [20, 21]. For their parallel counterparts, usually a different configuration of springs is used, and sometimes counterweights[20, 22, 23]. Gosselin carried out several studies on the gravity compensation of parallel robots and proposed a general mathematical formulation as a design tool for parallel mechanisms; however, the imposed limitations on achievable solutions reduced the number of feasible designs. The practicality of gravity compensation should therefore be improved through further research [21, 24]. Checcacci et al. adopted Lagrange's approach and screw theory for static balancing of a 5DOF parallel robot, and implied the experimental comparison of these two methods [25].

In this work we focus on a large workspace configuration of a 3-UPU parallel manipulator mounted in a horizontal configuration; we also present a particular solution for gravity compensation of this mechanism. The large size of this robot arises from the challenge of its gravity compensation. One contribution of the present work is to achieve the static balancing by a combination of mechanical and analytical compensation. As a mechanical compensation, two different configurations of springs are located along and orthogonal to the links (to the authors' knowledge there are no other 3-UPU mechanisms that use this spring configuration for gravity compensation). As an analytical compensation, based on Lagrange's approach we developed the gravity compensation algorithm for a horizontal 3-UPU parallel mechanism, for which we present both modelling and experimental performance characterization The Lagrange method is chosen to achieve a computationally efficient solution for this parallel robot. The reliability and effectiveness of the proposed algorithm is evaluated through experiment by employing a haptic interface and Virtual Reality (VR) environment. Due to the manipulator's task, which is carried out at low speed, the dynamic disturbance is negligible, and thus the dynamic balancing is not taken into account. The remainder of the paper is organized as follows. In section 2 the structure of our 3-UPU parallel manipulator is introduced and a brief description of its specific application in fMRI is given. Section 3 describes the proposed gravity compensation algorithm. The mechanical gravity compensation is discussed in section 4. The haptic experiment and discussion are presented in sections5 and 6 respectively. Finally, section 6 presents a conclusion.

2. Motivation

Parallel manipulators are known as mechanisms with complex direct kinematics. The available closed loops in these mechanisms make them more complicated compared to their serial counterparts in terms of

computations. The conventional Newton-Euler method which is now preferred for gravity compensation [21, 24], passes through the orientation matrices in order to represent each parameter with respect to another frame (or fixed frame). Thanks to the difficulty of mathematical computation of parallel mechanisms, this vector-based method leads to computationally expensive algorithms, much complexity and difficulties in obtaining solutions; feasible designs have therefore been limited. Therefore, an alternative is required in order to improve the practicality of balancing [20, 21, 24]. In this proposed method, based on the Lagrangian method a new algorithm is proposed. By obtaining the potential energy, we optimize the computational procedure. Thus, the potential gravitational and elastic energies are computed, and by taking account of the position of the end-effector the gravitational and elastic forces acting upon it are found in the Cartesian space. In order to provide gravity compensation for all of the configurations the total potential energy should be constant[21]. To demonstrate the effectiveness of the proposed algorithm, several experiments are carried out, as reported in section 5.

3. Device structure

A large number of stroke survivors lose motor control abilities in the brain. Functional magnetic resonance imaging, or fMRI, is a technique for measuring brain activity in neuroscience. Employing an fMRI-compatible robot and by providing a haptic application and virtual reality environment, a subject's motor interaction and the progress of therapy can be evaluated. In addition, daily life interactions and environments can be simulated, which can lead to the identification of the brain activity most similar to that during Activities of Daily Living (ADLs). In this project we designed and fabricated an fMRI-compatible horizontal 3-UPU parallel mechanism. It is important to provide precise control of the mechanism because of the crucial environment of the fMRI, and to guaranty the safety of the person during haptic interaction.

Figure 1 shows the 3D model of the designed mechanism and its application in fMRI. As can be seen, robot's end-effector should move with precision in the fMRI's narrow tunnel. Considering the strong magnetic field in the fMRI environment, in the fabrication of the robot magnetic-compatible materials are used. Carbon fibre with high stiffness is employed for the manufacturing of the comprehensive links. The rest of the device is made of polymers, and the parts exposed to high stresses are made of non-ferromagnetic metals such as aluminium and brass. In this 3-DOF manipulator, three shielded DC motors are used as link actuators. Electrical transmission happens through braid yarn cables. The robot is fixed to the aluminium supporting frame, which provides adjustability in the height and position of the device. In order to avoid affecting the brain image and ensure safety, the distance between the fMRI scanner and shielded motors should be more than 1. 8 m [26].

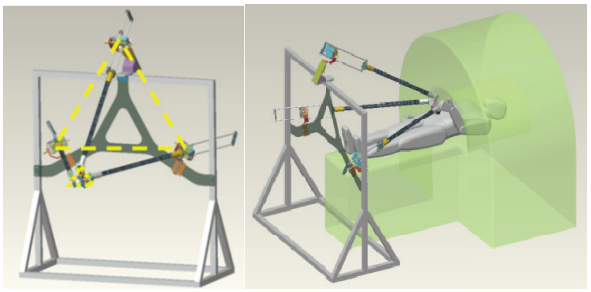

Figure 1. The 3D model of the 3-UPU parallel mechanism and fMRI scanner.

Figure 2 illustrates a schematic representation of the mechanism. As can be seen, the parallel manipulator consists of a fixed base, which is an isosceles triangle, and a moving platform, which is an equilateral triangle. The moving platform is magnified for clarity. These two triangular platforms are connected through three identical links, which are jointed to the planes by universal joints. Each universal joint is formed by two intersecting revolute joints. At the orthocentre of each triangular platform, a Cartesian coordinates is attached. The end-effector is fixed to the orthocentre of the moving platform with a small offset.

Due to the pure translational motion of the device, a geometric method is used to obtain the workspace of the manipulator [20]. Figure 3 shows the theoretical workspace of the device, which is the intersection of three spheres with a radius of the maximum link length. All of the dimensions are in metres. In practice, due to mechanical constraints, the manipulator's workspace becomes smaller.

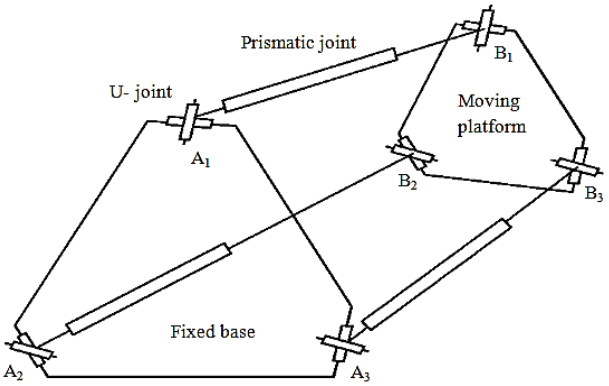

Figure 2. Schematic representation of the 3-UPU parallel mechanism.

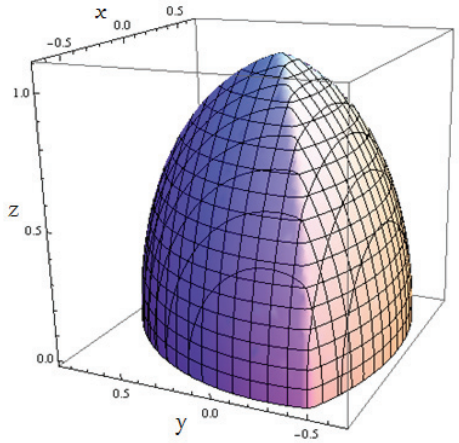

Figure 3. 3-UPU parallel mechanism's workspace.

4. Analytical gravity compensation

In the analytical study of parallel robots, the difficulty of achieving an accurate analysis of parallel mechanisms compared to their serial counterparts should be taken into account. In addition to the difficulty of computing a Jacobian matrix in the closed form, errors measurement and thermal errors can be problematic, as can manufacturing tolerances, etc. [24]. This section describes how to obtain the gravitational force imposed on the end-effector by exploiting the total potential energy of the system. Figure 4 shows the mechanism coordinates for a typical link. As can be seen at the orthocentre of each triangular platform, a Cartesian coordinate is attached. Point O is an orthocentre of the fixed base, and is defined as a base coordinate. At point O′, which is an orthocentre of the moving platform, a local coordinate is attached. $F_g$is a gravitational force at the end-effector, and F_i is a force introduced by the i^{th} actuator. Three components of $F_i$along axes of base coordinates are shown asF_{ix} , F_{iy}andF_{iz}.

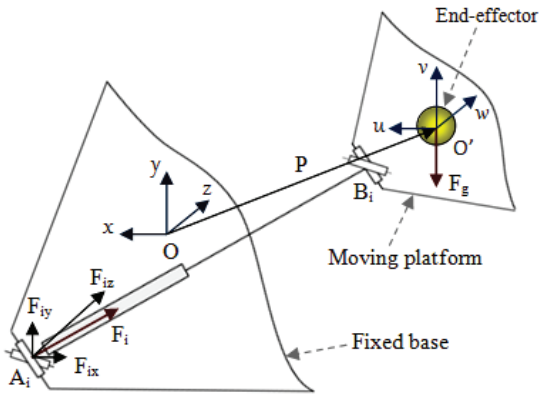

Figure 4. Mechanism's coordinates.

As discussed in reference [21], the position vector of the centre of mass of mechanism with respect to the Cartesian frame attached to the fixed base can be written as

$$c = \frac{1}{M}\sum_{i=1}^{n} m_i c_i \qquad (1)$$

where

n is a number of moving bodies in the mechanism;
m_i is the mass of i^{th} moving bodies;
M is the total mass of moving bodies, i. e.

$$M = \sum_{i=1}^{n} m_i \qquad (2)$$

In general, the position vector of centre of mass depends on the manipulator configuration. Defining λ as a vector composed of all the joint coordinates of themanipulator, c can be written as a function of λ as

$$\boldsymbol{c} = \boldsymbol{c}(\boldsymbol{\lambda}) \qquad (3)$$

The condition for the force balancing of the manipulator is

$$\boldsymbol{c} = \boldsymbol{c}_a \qquad (4)$$

where$\boldsymbol{c}_a$can be any arbitrary constant vector, i. e. , an independent vector from$\boldsymbol{\lambda}$.

The condition for statically balancing the mechanism in the absence of springs and other energy storing elements can be written as

$$\boldsymbol{e}_z^T \boldsymbol{c} = C_t \qquad (5)$$

where$\boldsymbol{e}_z$is a unit vector representing the direction of gravity and $C_t$can be anyarbitrary constant.

In the presence of elastic elements, the condition for static balancing is that the total potential energy of the system, which is the sum of gravitational and elastic potential energy, remains constant [21].

In order to find the centre of mass of a 3-UPU parallel manipulator, it is assumed that $P_x, P_y, P_z$are components of the position of the end-effector $\boldsymbol{P}$ in relation to the base coordinate, as shown in Figure 4. For this mechanism, seven moving bodies are considered, six for three links and one for the end-effector, where two centres of mass at each link refer to the carbon beam and the aluminium bars that form the link and actuator, respectively. In this manipulator, $\boldsymbol{e}_z$ works along the y-axis of the defined Cartesian space. Solving *Direct Kinematics* and *Inverse Kinematics*, link length d and the position of the end-effector **P** are known in any configuration [5].

Projecting the three links and the end-effector on the x-y plane of the base coordinate, the position of centres of mass along the y-axis can be obtained as

$$\varphi_i = \cos^{-1}\left(\frac{P_z}{d_i}\right) \quad i = 1, 2, 3 \qquad (6)$$

$$\psi_1 = \cos^{-1}\left(\frac{P_x}{d_1 \sin\varphi_1}\right) \quad (7)$$

$$\psi_i = \sin^{-1}\left(\frac{|\alpha + P_y|}{d_i \sin\varphi_i}\right) \quad 2,3 \quad (8)$$

$$C_{c1} = P_y + L_{g1} \sin\varphi_1 \sin\psi_1 \quad (9)$$

$$C_{ci} = P_y - L_{gi} \sin\varphi_i \sin\psi_i \quad i = 2,3 \quad (10)$$

$$C_{Al1} = P_y + L_{Al1} \sin\varphi_1 \sin\psi_1 \quad (11)$$

$$C_{Ali} = P_y - L_{Ali} \sin\varphi_i \sin\psi_i \quad i = 2,3 \quad (12)$$

where

φ_i is an angle between the x-axis and the projection of the ith link on the fixed base.
$d_i$is a length of the ith link.
P_x, P_y and P_z are components of the position of the end-effector in the Cartesian coordinates.
ψ_i is an angle between the ith link and z-axis.
α is a constant referring to the fixed base triangular structure.
C_{ci} is the position of the centre of mass of the carbon beam of the ith link along the y-axis.
C_{Ali} is the position of the centre of mass of the aluminium bars of the ith prismatic joint along the y-axis.
L_{gi} is the distance between the centre of mass of the carbon beam of the ith link and the end-effector.
L_{Ali} is the distance between the centre of mass of the aluminium bars of the ith prismatic joint and the end-effector.

Therefore, the gravitational potential energy of the system can be written as

$$U_g = g e_z^T \sum_{i=1}^{n} m_i c_i \quad (13)$$

where n=7 and g is the magnitude of the gravitational acceleration.

Without loss of generality, one can obtain:

$$u = [M_{ee} M_1 M_2 M_3 M_{Al1} M_{Al2} M_{Al3}] \cdot \begin{bmatrix} P_y & & & \dots & & & 0 \\ & C_{c1} & & & & & \\ & & C_{c2} & & & & \\ \vdots & & & C_{c3} & & & \vdots \\ & & & & C_{Al1} & & \\ & & & & & C_{Al2} & \\ 0 & & & \dots & & & C_{Al3} \end{bmatrix} \quad (14)$$

where $\boldsymbol{M_{ee}}$, $\boldsymbol{M_i}$ and $\boldsymbol{M_{Ali}}$ are matrices of size 3×1, which are masses of end-effector, link i and aluminium bars of ith prismatic joint, respectively, for i=1, 2, 3.

Therefore, the total potential energy of the system can be obtained as a function of **P** as follows:

$$U_g = g \boldsymbol{e_z^T} u \boldsymbol{\kappa} \quad (15)$$

where κ is an arbitrary constant vector of size 7 × 1.

Deriving from [25] the gravitational force can be written as

$$\boldsymbol{F} = \lim_{\Delta P \to 0} \frac{\Delta U(\boldsymbol{P})}{\Delta \boldsymbol{P}} = \frac{\partial U(\boldsymbol{P})}{\partial \boldsymbol{P}} \quad (16)$$

Assume $\mathbf{F_g}$ and $\mathbf{F_m}$ are gravitational and motor forces, respectively, working on the end-effector. The condition for gravity compensation can now be written as

$$F_g + F_m + f' = C_f \quad (17)$$

where f' represents the disturbances existing in the system and $C_f$is an arbitrary constant.

Following the notation, gravitational force at the end-effector in the Cartesian space can be obtained as

$$\Lambda = \frac{\partial U}{\partial \varphi} = \begin{bmatrix} \frac{\propto_1 \cos\varphi_1 (P_y - \alpha_2)}{\sqrt{P_x^2 + (P_y - \propto_2)^2}} \\ \frac{\propto_1 \cos\varphi_2 (P_y + \alpha_3)}{P_z^2 + \sqrt{(P_x + \propto_4)^2 + (P_y + \propto_5)^2 + P_z^2}} \\ \frac{\propto_1 \cos\varphi_3 (P_y + \alpha_3)}{P_z^2 + \sqrt{(P_x - \propto_4)^2 + (P_y + \propto_5)^2 + P_z^2}} \end{bmatrix}^T \quad (18)$$

where $\propto_i$ are constants conditional on device structural properties; and

$$\mathrm{X} = \frac{\partial \varphi}{\partial \boldsymbol{P}} = \begin{bmatrix} \frac{P_z P_x}{E_1^{3/2}(1 - \frac{P_z^2}{E_1})^{1/2}} & \dots & 0 \\ \vdots & \frac{\beta_1 P_z (\beta_2 P_x + \beta_3)}{E_2^{3/2}(1 - \frac{P_z^2}{E_2})^{1/2}} & \vdots \\ 0 & \dots & \frac{\beta_1 P_z (\beta_2 P_x - \beta_3)}{E_3^{3/2}(1 - \frac{P_z^2}{E_3})^{1/2}} \end{bmatrix} \quad (19)$$

where

$$E_1 = P_x^2 + (P_y + \gamma_0)^2 + P_z^2 \quad (20)$$

$$E_2 = (P_x + \gamma_1)^2 + (P_y + \gamma_2)^2 + P_z^2 \quad (21)$$

$$E_3 = (P_x - \gamma_1)^2 + (P_y + \gamma_2)^2 + P_z^2 \quad (22)$$

Where β_i s and γ_i s are constants whose values are obtained based on device structural properties.

Therefore, $\boldsymbol{F_g}$, the gravitational force on the end-effector, can be obtained in terms of P as follows:

$$\boldsymbol{F}_g = \Lambda \, \mathrm{X} = \frac{\partial U}{\partial \varphi}\frac{\partial \varphi}{\partial \boldsymbol{P}} = \begin{bmatrix} F_x(P_x, P_y, P_z) \\ F_y(P_x, P_y, P_z) \\ F_z(P_x, P_y, P_z) \end{bmatrix} \quad (23)$$

where F_x, F_y and F_z are components of $\boldsymbol{F}_g$ along the x-axis, y-axis and z-axis respectively, and are functions of the position of the end-effector.

5. Mechanical gravity compensation

In order to decrease the burden of actuators, to provide gravity compensation elastic components, e. g. , springs, can be used. Elastic components are also able to provide balancing conditions even in the absence of actuator force; for an example, see [23].

In the presence of springs, gravity compensation refers to the set of conditions where the total potential energy of the mechanism is constant for any configuration of the manipulator [21]. These conditions can be written as

$$U = C_e \quad (24)$$

where Ce is an arbitrary constant.

The total potential energy of the system is given bythe summation of gravitational potential energy and elastic potential energy stored in the springs [21], which can be written as

$$U = g\boldsymbol{e}_z^T \sum_{i01}^{n_b} m_i c_i + \frac{1}{2}\sum_{j=1}^{n_s} k_j \left(L_j - L_{j0}\right)^2 \quad (25)$$

where

n_s is the number ofthe mechanism's linear elastic elements,
k_j is the stiffness of the j[th] elastic element,
L_j is the length of the j[th] elastic element,
L_{j0} is the undeformed length of the j[th] elastic element.

The literature shows that in order to provide gravity compensation, several combinations of springs should be used [20, 22]. Springs are mostly used because they impose negligible mass and inertia on the mechanism. In this work, two systems of springs are designed. The first is designed to place springs along the mechanism's links (corresponding to the prismatic joints' movements) in order to decrease the burden of the actuators; the second is designed to connect the centre of mass of each link to the fixed point, in such a way that springs are placed nearly orthogonal to the ground. This system of springs thus provides vertical force (against gravitational force) and plays the most important role in the gravity compensation.

The elastic potential energy of the springs can be written as

$$U_{es} = \frac{1}{2}\sum_{i=1}^{3}(k_{li}\Delta L_{li}^2 + k_{vi}\Delta L_{vi}^2) \quad (26)$$

where for i=1, 2, 3, k_i is the stiffness of the springs, ΔL_i is the variation in the spring's length from its undeformed length, l stands for springs which are placed along mechanism links, and v stands for springs that are placed nearly vertically.

To compute the total elastic forces, first we calculate the force provided by springs along mechanism links, and then the force introduced by springs that are placed nearly orthogonally to the ground. Figure 5 shows the schematic representation of one typical link with the spring attached along a prismatic joint.

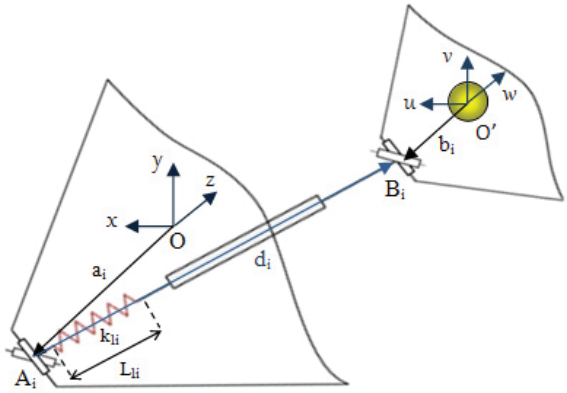

Figure 5. Schematic representation of a typical joint with spring.

Let $\boldsymbol{a}_i$ and $\boldsymbol{b}_i$ be the position vectors of points A_i and B_i in relationto the coordinate attached to the fixed and moving platform, respectively (see Figure 5). As addressed in [5], s_i, a unit vector of the i[th] limb pointing along the prismatic joint, can be written as

$$\boldsymbol{s}_i = \left[\frac{P_x - e_{ix}}{d_i}, \frac{P_y - e_{iy}}{d_i}, \frac{P_z - e_{iz}}{d_i}\right] \quad i = 1, 2, 3 \quad (27)$$

where

$$\boldsymbol{e}_i = \boldsymbol{a}_i - \boldsymbol{b}_i \quad i = 1, 2, 3 \quad (28)$$

Following this notation, the length of spring in any configuration can be written as

$$L_{li} = d_i - L_{ci} \quad i = 1, 2, 3 \quad (29)$$

where constant value L_{ci} is the length of the fixed part of the i[th] limb, and, as mentioned, d_i is the length of the i[th] limbs, which is known from inverse kinematics.

Hence, the spring's length variation can be written as

$$\Delta L_{li} = L_{li} - L_{l0i} = d_i - L_{ci} - L_{l0i} \quad i = 1, 2, 3 \quad (30)$$

whereL_{l0i} is the undeformed length of the i[th] limb's spring.

Let $\Delta \boldsymbol{x}_i$ be the vector of length variation. One can obtain this vector as

$$\Delta \boldsymbol{x}_{li} = \Delta L_{li}.\boldsymbol{s}_i^T \quad i = 1,2,3 \tag{31}$$

The spring force can be written as

$$\boldsymbol{F}_{lsi} = k_{li}.\Delta \boldsymbol{x}_{li} \quad i = 1,2,3 \tag{32}$$

In order to obtain the force imposed by the springs on the end-effector, equation 16 is used as a new alternative. In this way, by taking a derivative of spring potential energy with respect to the position of the end-effector, the force on the end-effector due to the springs in the Cartesian space is obtained, and can be written as

$$\boldsymbol{F}_{els} = \frac{\partial U_{els}}{\partial \boldsymbol{P}} \tag{33}$$

$$\boldsymbol{F}_{els} = \begin{bmatrix} -k_{l1}\frac{P_x \mathrm{K}_1}{D_1^{1/2}} + k_{l2}\frac{(P_x+\xi_3)\mathrm{K}_2}{D_2^{1/2}} + k_{l3}\frac{(P_x-\xi_3)\mathrm{K}_3}{D_3^{1/2}} \\ -k_{l1}\frac{(P_y-\xi_4)\mathrm{K}_1}{D_1^{1/2}} + k_{l2}\frac{(P_y+\xi_5)\mathrm{K}_2}{D_2^{1/2}} + k_{l3}\frac{(P_y+\xi_5)\mathrm{K}_3}{D_3^{1/2}} \\ -k_{l1}\frac{P_z \mathrm{K}_1}{D_1^{1/2}} + k_{l2}\frac{P_z \mathrm{K}_2}{D_2^{1/2}} + k_{l3}\frac{P_z \mathrm{K}_3}{D_3^{1/2}} \end{bmatrix} \tag{34}$$

where

$$\mathrm{K}_1 = -D_1^{1/2} + \xi_1 - L_{l01} \tag{35}$$

$$\mathrm{K}_2 = D_2^{1/2} - \xi_2 - L_{l02} \tag{36}$$

$$\mathrm{K}_3 = D_3^{1/2} - \xi_2 - L_{l03} \tag{37}$$

and

$$D_1 = P_x^2 + \left(P_y - \xi_4\right)^2 + P_z^2 \tag{38}$$

$$D_2 = (P_x + \xi_3)^2 + \left(P_y + \xi_5\right)^2 + P_z^2 \tag{39}$$

$$D_3 = (P_x - \xi_3)^2 + \left(P_y + \xi_5\right)^2 + P_z^2 \tag{40}$$

and ξ_i are the mechanism's instructional constants. In order to obtain F_{elC}, the force of the spring on the end-effector in the Cartesian space, taking advantage of Jacobian matrix (addressed in [5]), one can write

$$\boldsymbol{J} = \begin{bmatrix} s_1^T \\ s_2^T \\ s_3^T \end{bmatrix} \tag{41}$$

$$\boldsymbol{F}_{elC} = \boldsymbol{J}^T.\boldsymbol{F}_{els} = \begin{bmatrix} F_{elx}(P_x,P_y,P_z) \\ F_{ley}(P_x,P_y,P_z) \\ F_{elz}(P_x,P_y,P_z) \end{bmatrix} \tag{42}$$

where F_{elx}, F_{ely} and F_{elz} are components of F along the x-axis, y-axis and z-axis, respectively, and are functions of the position of the end-effector.

After obtaining the force provided by the link springs, the force of the second system of springs is computed. In this system each spring connects the centre of mass of the link to the related extended bar, which is fixed to the mechanism's supporting frame. Figure 6 shows the schematic representation of a vertical spring attached to a typical link.

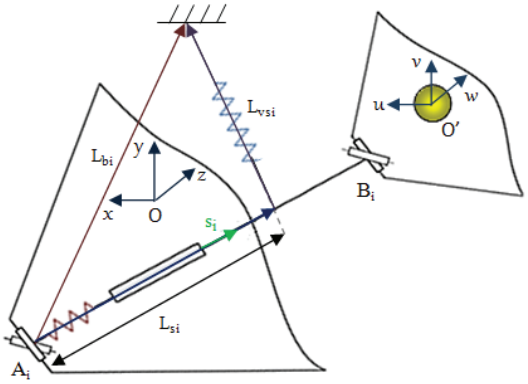

Figure 6. Schematic representation of a typical link with vertical spring.

Let L_{bi} be the vector pointing from A_i to the upper end of the spring and let L_{si} be the distance between A_i and the lower end of the spring (centre of mass of the link). L_{vsi}, the vector of the spring length, can then be written as

$$L_{vsi} = L_{bi} - L_{si}.s_i^T \quad i = 1,2,3 \tag{43}$$

Thus, L_{ni}, the length of the spring, can be obtained as

$$L_{ni} = \sqrt{L_{vsi}^2(x) + L_{vsi}^2(y) + L_{vsi}^2(z)} \quad i = 1,2,3 \tag{44}$$

Following this notation, the v_{si}, a unit vector of the length variation of the i^{th} vertical spring, can be written as

$$v_{si} = \frac{L_{vsi}}{L_{ni}} \quad i = 1,2,3 \tag{45}$$

Let ΔL_{vi} be the length variation of i^{th} spring; one can then obtain

$$\Delta L_{vi} = L_{ni} - L_{v0i} \quad i = 1,2,3 \tag{46}$$

where L_{v0i} is the undeformed length of the i^{th} vertical spring.

Thus, Δx_{vi}, the vector of the i^{th} vertical spring length variation, can be written as

$$\Delta x_{vi} = \Delta L_{vi}.v_{si} \quad i = 1,2,3 \tag{47}$$

Therefore, the vertical spring force can be written as

$$\boldsymbol{F}_{vs} = k_{vi}.\Delta \boldsymbol{x}_{vi} \quad i = 1,2,3 \tag{48}$$

In order to obtain the force imposed on the end-effector due to the system of vertical springs, the same computation as for the link's spring is done using equation 16. Thus, this force in the Cartesian space can be obtained as

$$\boldsymbol{F}_{evs} = \frac{\partial U_{evs}}{\partial \boldsymbol{P}} = \frac{\partial U_{evs}}{\partial \boldsymbol{s}} \frac{\partial \boldsymbol{s}}{\partial \boldsymbol{P}} \tag{49}$$

and

$$\Omega = \frac{\partial \boldsymbol{s}}{\partial \boldsymbol{P}} = \begin{bmatrix} \frac{1}{\theta_1^{1/2}} - \frac{P_x^2}{\theta_1^{3/2}} & -\frac{P_x(P_y-\varrho_0)}{\theta_1^{3/2}} & -\frac{P_z P_x}{\theta_1^{3/2}} \\ \frac{1}{\theta_2^{1/2}} - \frac{(P_x+\varrho_1)^2}{\theta_2^{3/2}} & -\frac{(P_x+\varrho_1)(P_y+\varrho_2)}{\theta_2^{3/2}} & -\frac{P_z(P_x+\varrho_1)}{\theta_2^{3/2}} \\ \frac{1}{\theta_3^{1/2}} - \frac{(P_x-\varrho_1)^2}{\theta_3^{3/2}} & -\frac{(P_x-\varrho_1)(P_y+\varrho_2)}{\theta_3^{3/2}} & -\frac{P_z(P_x-\varrho_1)}{\theta_3^{3/2}} \end{bmatrix} \tag{50}$$

where

$$\Theta_1 = P_x^2 + (P_y - \varrho_0)^2 + P_z^2 \tag{51}$$

$$\Theta_2 = (P_x + \varrho_1)^2 + (P_y + \varrho_2)^2 + P_z^2 \tag{52}$$

$$\Theta_3 = (P_x - \varrho_1)^2 + (P_y + \varrho_2)^2 + P_z^2 \tag{53}$$

and

$$\Upsilon = \frac{\partial U_{ev}}{\partial \boldsymbol{s}} = \begin{bmatrix} \frac{k_{v1}\Gamma_1\Phi_1(3\Gamma_1 s_1 - \mu_0)\left(\Phi_1^{1/2} - L_{v01}\right)}{\Phi_1^{1/2}} \\ \frac{k_{v2}\Gamma_2(3\Gamma_2 s_2 - \mu_1)\left(\Phi_2^{1/2} - L_{v02}\right)}{\Phi_2^{1/2}} \\ \frac{k_{v3}\Gamma_3(3\Gamma_3 s_3 - \mu_2)\left(\Phi_3^{1/2} - L_{v03}\right)}{\Phi_3^{1/2}} \end{bmatrix} \tag{54}$$

where

$$\Phi_1 = \Gamma_1^2 s_1^2 + (\Gamma_1 s_1 + \mu_3)^2 + (\Gamma_1 s_1 + \mu_4)^2 \tag{55}$$

$$\Phi_2 = (\Gamma_2 s_2 - \mu_5)^2 + (\Gamma_2 s_2 - \mu_6)^2 + (\Gamma_2 s_2 - \mu_7)^2 \tag{56}$$

$$\Phi_3 = (\Gamma_3 s_3 + \mu_5)^2 + (\Gamma_3 s_3 - \mu_6)^2 + (\Gamma_3 s_3 - \mu_7)^2 \tag{57}$$

and

$$\Gamma_1 = \left(P_x^2 + \left(P_y - \varrho_0\right)^2 + P_z^2\right)^{1/2} - \xi \tag{58}$$

$$\Gamma_2 = \left((P_x + \varrho_1)^2 + \left(P_y + \varrho_2\right)^2 + P_z^2\right)^{1/2} - \xi \tag{59}$$

$$\Gamma_3 = \left((P_x - \varrho_1)^2 + \left(P_y + \varrho_2\right)^2 + P_z^2\right)^{1/2} - \xi \tag{60}$$

Following the notation, one can therefore obtain

$$\boldsymbol{F}_{evs} = \Omega\Upsilon = \frac{\partial U_{ev}}{\partial s}\frac{\partial s}{\partial P} = \begin{bmatrix} F_{evx}(P_x, P_y, P_z) \\ F_{evy}(P_x, P_y, P_z) \\ F_{evz}(P_x, P_y, P_z) \end{bmatrix} \tag{61}$$

where F_{evx}, F_{evy} and F_{evz} are three components of $\boldsymbol{F}_{evs}$ in the Cartesian space, and are functions of the position of the end-effector in relation to the based coordinate.

In order to provide gravity compensation, the following condition should be satisfied:

$$F_{elC} + F_{evs} + F_m + F_g + f' = C_\tau \tag{62}$$

where C_τ is an arbitrary constant and is equal to zero in a complete compensation. In articulated mechanical systems the gravitational force may be compensated completely by elastic components (e. g. , springs) for all configurations. Thus, the gravity compensation condition can be written as

$$F_{elC} + F_{evs} + F_g + f' = C_g \tag{63}$$

where C_g is an arbitrary constant and, in a complete compensation, is equal to zero.

6. Experimental Test

In order to evaluate the effectiveness and reliability of the proposed model, several experiments were carried out, with and without springs. During the experiments a force sensor was attached to the end-effector of the robot and measured the gravitational force imposed on the end-effector. The sensitivity and rated capacity of the force sensor were 10, 015[V] and 245, 166[N], respectively. Employing XVR (eXtreme Virtual Reality, VRMedia ®), the virtual reality application was carried out, whereby a virtual room was designed. A small ball was placed in the virtual room as an indicator of the end-effector's position; the end-effector pursues its movement in the virtual reality environment. The experimental works are classified as two experiments: in the first experiment, no elastic components were used, while in the second a spring was attached along the first link, and two vertical springs were fixed to the second and third links in order to impose vertical forces against gravitational force. Figure 7 shows the 3-UPU parallel mechanism with attached springs.

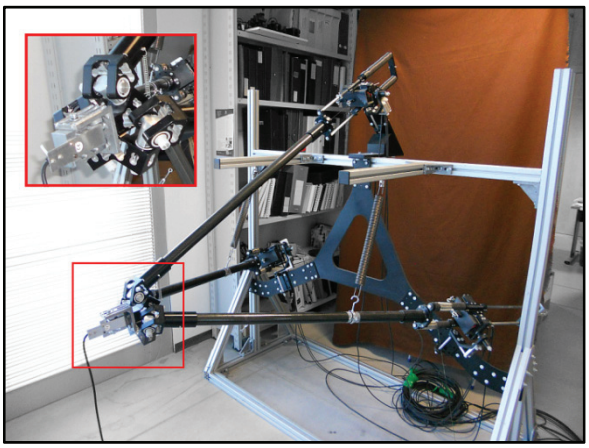

Figure 7. Horizontal 3-UPU parallel mechanism with elastic elements.

6. 1 System without elastic elements

The first experiment aimed to evaluate the effectiveness and reliability of the modelling and analytical gravity compensation algorithm. As can be seen in Figure 8 (a), six yellow balls were placed in the virtual room in different trial positions of the same plane in the symmetric pattern, along the x and z axes. This pattern was chosen in order to observe and compare the mechanism's behaviour in the symmetrical configuration of the limbs and in the symmetrical points. The subject was asked to hold and move the end-effector of the 3-UPU parallel mechanism to place the end-effector indicator (red ball) on the positions of the yellow balls one by one. In order to minimize the disturbance imposed by subject and environment, we saved the data from sensor and model while the force sensor was fixed to a table. Figure 8 (b) illustrates the position of the end-effector in each trial position in the mechanism workspace. For each position, based on the gravity compensation algorithm, the combination of actuators' forces imposed the force along the y-axis on the end-effector, which led to the static balancing. The real weight of the device for any position is measured using a force sensor.

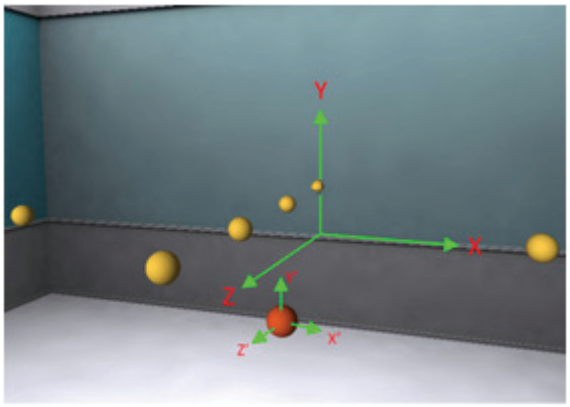

(a)

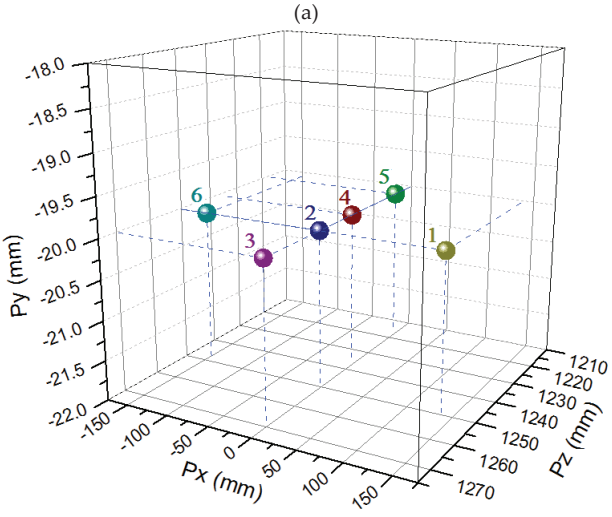

(b)

Figure 8. (a) Trial points' positions in the virtual reality application; (b) Positions of the end-effector in the workspace.

Figure 9 shows the comparison of the forces measured from sensors and the value obtained from the model along the y-axis. The maximum observed error was equal to 2. 09 [N].

For gravity compensation of a vertical configuration parallel robot, an almost symmetrical distribution of forces is expected among different links; however, in this horizontal configuration we observed a greater force on the first link, which means the first actuator should produce more force. The actuators' currents, applied to provide gravity compensation on each trial position, are illustrated in Figure 10. As can be seen, the current of the first actuator is about twice that of the other actuators, showing that most of the gravity compensation came from the first actuator. This should be carefully analysed, since it limits the overall performance of the mechanism.

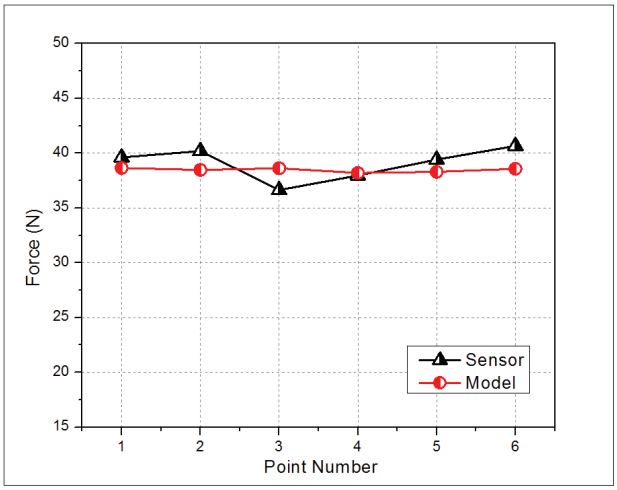

Figure 9. Comparison of forces obtained from model and sensor in the absence of elastic elements.

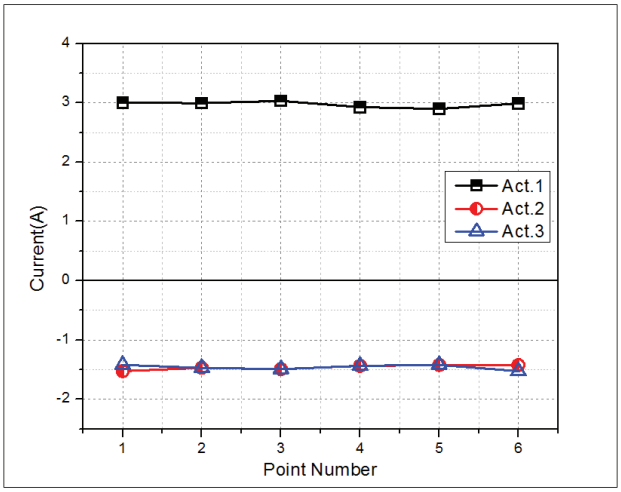

Figure 10. Actuators' currents in the absence of elastic elements.

6. 2 System with elastic elements

In this experiment, in order to satisfy gravity compensation conditions in the absence of actuators, a configuration of springs was attached to the mechanism. A compression spring with as tiffness of 0. 03 [N/mm] and an undeformed length of 1100 mm was attached along the first link, while two extension springs with stiffness and undeformed length of 0. 2 [N/mm] and 350 mm were fixed to the centre of mass of the second and third links (see Figure 7). Employing the above-mentioned XVR application and attaching the force sensor to the end-effector, the previous experiment was repeated by the subject, and the data for each trial point were preserved. Figure 11 shows the actuator currents relevant to each trial point. As can be seen, the currents of all three actuators, especially the first one, were decreased dramatically, and the gravitational force was distributed among the three links symmetrically.

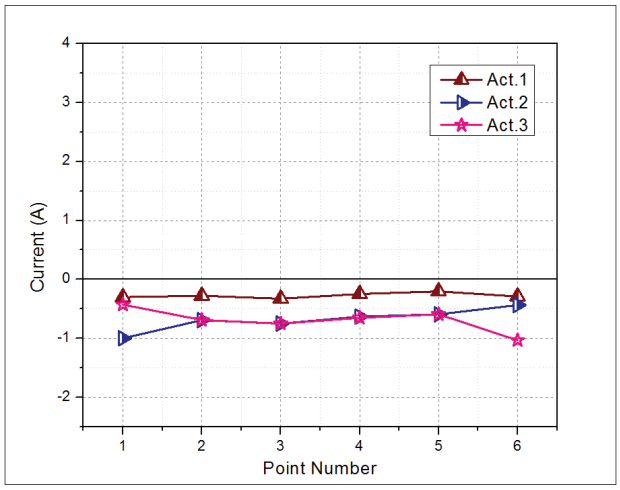

Figure 11. Actuators' currents in the existence of elastic elements.

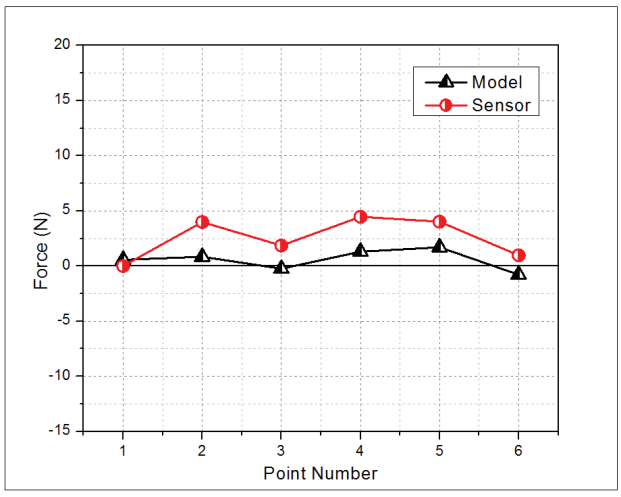

Figure 12. Comparison of forces obtained from model and sensor in the existence of elastic elements.

In this experiment, the force produced by the system of springs compensated the gravitational force; the low current of the actuator was due to adjusting undesirable spring forces along the x and z axes. Figure 12 illustrates the force measured by the sensor and the force obtained from the model. In the existence of the springs the maximum observed error was equal to 3. 158[N].

7. Discussion

The gravity compensation experiments were carried out successfully and the mechanism remains statistically balanced for the whole workspace including the mentioned trial points, which demonstrates the correctness of the gravity compensation algorithm. In addition, by implementing a system of three springs, in the absence of actuators the manipulator had a static balancing, while the links were at their minimum length and the end-effector was along the z-axis. The fact that the experimental force read by the sensor is not the same as that of model could be clearly explained by the presence of many sources of unmodelled properties (mainly static and dynamic friction) or uncertainties with the modelled ones (masses, parts dimensions).

The experimental results indicate that using elastic elements successfully led to a decrease in the burden of actuators to compensate the mechanism's weight when the system is statically balanced, even in the absence of actuators. Figure 13 shows the percentage of the reduction of the actuators' absolute current for each trial position. As can be seen, the most-observed effect of employing springs was with the first actuator, where current was decreased to 3. 36 A. Comparison of Figures 10 and 11 demonstrates that the proposed spring configuration allowed a symmetrical distribution of gravity compensation forces among the three actuators to be achieved, which improved the performance of the mechanism.

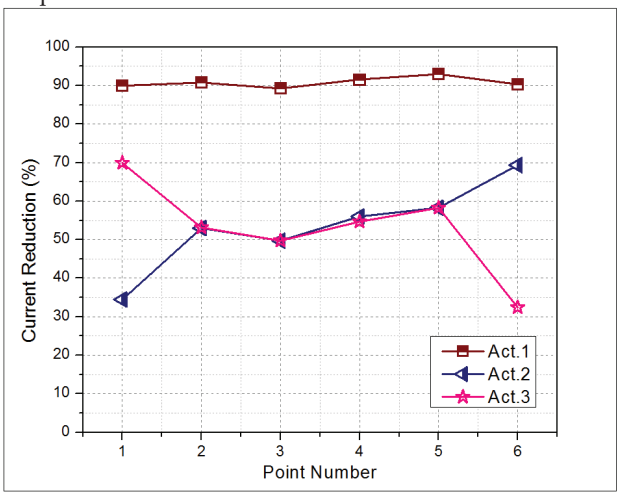

Figure 13. The percentage of the actuators' current reduction due to the existence of elastic elements.

8. Conclusions

The conventional Newton-Euler approach to static balancing works for serial robots, but it shows some weaknesses applied to their parallel counterparts. In this paper anew algorithm for gravity compensation in a horizontal 3-UPU parallel mechanism was presented. The proposed algorithm is based on a Lagrangian model and takes advantage of the total potential energy of the system. It has been discussed in terms of analytical (mechanism weight compensated by actuator forces) and mechanical (employing three springs configuration) approaches. To evaluate the effectiveness of both analytical and mechanical algorithms, several experiments were carried out in the presence and absence of springs.

The feasibility and reliability of this model have been successfully demonstrated for a horizontal 3-UPU parallel mechanism. The proposed algorithm can be implemented for any parallel mechanism, knowing the total potential energy of the system and the position of the end-effector. The observed error between model and measured force was due to friction and other sources of uncertainties, which will be taken into the account in future work.

9. Acknowledgements

This research was carried out with the financial support of the BRAVO and VERE projects.

10. References

[1] Yang Z, Wu J, Mei J, Gao J, Huang T (2008) Mechatronic model based computed torque control of a parallel manipulator. International Journal of Advanced Robotic Systems, 5(1):123-28.

[2] Fried G, Djouani K, Fijany A (2012) Kinematic and Inverse Dynamic Analysis of a C5 Joint Parallel Robot. In: Dutta A, editor. Robotic Systems – Applications, Control and Programming. InTech. pp. 339-360.

[3] Wu H, Handroos H, Pessi P (2008) Hybrid Parallel Robot for the Assembling of ITER. In: Wu H, editor. Parallel Manipulators, towards New Applications. InTech. pp. 363-378.

[4] Gallardo-Alvarado J (2009) Jerk Analysis of the Spine by Means of a Parallel Manipulator. International Journal of Advanced Robotic Systems. 6(4):337-342.

[5] Tsai L. W, Joshi S (2000) Kinematics and Optimization of a Spatial 3-UPU Parallel Manipulator. ASME Journal of Mechanical Design. 122: 439–446.

[6] Joshi S, Tsai L. W (2002) Jacobian Analysis of Limited-DoF Parallel Manipulators. ASME Transactions, Journal of Mechanical Design. 124(2): 254–258.

[7] Frisoli A, Checcacci D, Salsedo F, Bergamasco M (2000) Synthesis by screw algebra of translating in-parallel actuated mechanisms. Proceedings of the ARK2000 7th International Symposium on Advances in Robot Kinematics. pp. 433–440.

[8] Han C, Kim J, Kim J, Park F. C (2002) Kinematic sensitivity analysis of the 3-UPU parallel mechanism. Mechanism and Machine Theory. 37(8): 787-798.

[9] Walter D. R, Husty M. L, Pfurner M (2008)The SNU 3-UPU Parallel Robot from a Theoretical Viewpoint. Proceedings of the Second International Workshop on Fundamental Issues and Future Research Directions for Parallel Mechanisms and Manipulators. pp. 1-8.

[10] Wolf A, Shoham M, Park F. C (2002) Investigation of Singularities and Self-Motions of the 3-UPU Robot. In: Lenarčič J, Thomas F, editors. Advances in Robots Kinematics: Theory and Applications. Kluwer Academic Publishers. Norwell, MA. pp. 165–174.

[11] Liu G, Lou Y, Li Z (2003) Singularities of Parallel Manipulators: A Geometric Treatment. IEEE Transactions on Robotics and Automation 19(4): 579-594.

[12] Walter D. R, Husty M. L, Pfurner M (2009) A complete kinematic analysis of the SNU 3-UPU parallel robot. In: Bates D. J, Besana G. M, Di Rocco S, Wampler C. W, editors. Interactions of Classical and Numerical Algebraic Geometry. Proceeding of a conference in honor of AJ Sommese, Notre Dame. Volume Contemporary Mathematics 496, pp. 331– 346.

[13] Di Gregorio R, Parenti-Castelli V (2002) Mobility analysis of the 3-UPU parallel mechanism assembled for a pure translational motion. ASME J. Mech. Des. , 124:259–264.

[14] Alici G, Shirinzadeh B (2006) Optimum Dynamic Balancing of Planar Parallel Manipulators Based on Sensitivity Analysis. Mechanism and Machine Theory, 41(12):1520–1532.

[15] Van der Wijk V, Herder J. L. (2009) Comparison of Various Dynamic Balancing Principles Regarding Additional Mass and Additional Inertia. Journal of Mechanisms and Robotics , 1(4):1-9.

[16] Lee S. H. , Kim B. S. et al. (2005) A Study on Active Balancing for Rotating Machinery Using Influence Coefficient Method, " in Proceedings of 2005 IEEE International Symposium on Computational Intelligence in Robotics and Automation, Espoo, Finland, pp. 659-664.

[17] Kochev I. S. (1990) General Method for Active Balancing of Combined Shaking Moment and Torque Fluctuations in Planar Linkages, Mechanism and Machine Theory, 25(6): 679–687.

[18] Thuemmel T (1995) Dynamic Balancing of Linkages by Active Control With Redundant Drives. In: Proceedings of the Ninth World Congress of the Theory of Machines and Mechanisms, pp. 970–974.

[19] Acevedo M, Ceccarelli M, Carbone G (2012) Application of Counter-Rotary Counterweights to the Dynamic Balancing of a Spatial Parallel Manipulator. Applied Mechanics and Materials, 162:224–233.
[20] Siciliano B, Khatib O (2008) Springer Handbook of Robotics. Springer Berlin Heidelberg.
[21] Gosselin C (2008) Gravity compensation, static balancing and dynamic balancing of parallel mechanisms. In: Wang L, Xi J, editors. Smart Devices and Machines for Advanced Manufacturing. Springer London, pp. 27-48.
[22] Wang L, Xi J (2008) Smart devices and machines for advanced manufacturing . Springer London.
[23] Deepak S. R, Ananthasuresh G. K (2012)Static balancing of a four-bar linkage and its cognates. Mechanism and Machine Theory, 48:62-80.
[24] Merlet J. P, Gosselin C (2008) Parallel mechanisms and robots. In:Siciliano B, Khatib O, editors. Springer Handbook of Robotics. Springer Berlin Heidelberg, pp. 269–285.
[25] Checcacci D, Sotgiu E, Frisoli A, Avizzano C, Bergamasco M (2002) Gravity compensation algorithms for parallel haptic interface. In: Robotand Human Interactive Communication. Proceedings. 11th IEEE International Workshop on, pp. 140–145.
[26] Li S, Frisoli A, Solazzi M, Bergamasco M (2010) Mechanical design and optimization of a novel fMRI compatible haptic manipulator. In: ROMAN, IEEE. pp. 1–6.